International Journal of Advanced and Applied Sciences, 12(11) 2025, Pages: 19-28

Contents lists available at Science-Gate

International Journal of Advanced and Applied Sciences

Journal homepage: http://www.science-gate.com/IJAAS.html

Lung cancer pathological image classification using spatial-channel attention (SCA) mechanism

Siran Zhong [1, 2], Qin Peng [3], Fan Zhang [4], Wen Lin [2], Kanakarn Phanniphong [5, *]

[1]*Chakrabongse Bhuvanarth International College for Interdisciplinary Studies, Rajamangala University of Technology Tawan-ok, Bangkok, Thailand*
[2]*Faculty of Data Science, Guangzhou Huashang College, Guangzhou, China*
[3]*Faculty of Data Science, City University of Macau, Macau, China*
[4]*Shenzhen Bao'an Chinese Medicine Hospital, Guangzhou University of Chinese Medicine, Shenzhen, China*
[5]*Faculty of Business Administration and Information Technology, Rajamangla University of Technology Tawan-ok, Bangkok, Thailand*

ARTICLE INFO

Article history:
Received 11 February 2025
Received in revised form
23 June 2025
Accepted 9 October 2025

Keywords:
Lung cancer
Deep learning
Pathology images
Image classification
Diagnostic accuracy

ABSTRACT

With the increasing use of deep learning in medical imaging, particularly in analyzing lung cancer pathology images, this technology shows great promise for building models for pathological grading and prognosis. This study highlights the growing importance of deep learning in this area, but also notes that accurately classifying lung cancer pathology images remains a difficult task, especially when high precision is needed for grading and prognosis. The aim of this research is to improve the classification of lung cancer pathology images by developing and optimizing a deep learning model. The study focuses on comparing different models, with special attention given to improving the performance of the SCA-ResNet model. The results show that SCA-ResNet performs better than the commonly used ResNet-50 model. It achieves higher scores in several evaluation measures, including precision, recall, specificity, F1 score, and the Kappa coefficient. ROC curve analysis also supports the superior performance of SCA-ResNet, showing better diagnostic accuracy across different cancer grades. These findings suggest that the SCA-ResNet model can offer more accurate and reliable classification of lung cancer pathology images, which may help doctors make better decisions about treatment and prognosis. Its use in clinical practice could lead to improved diagnostic accuracy and better outcomes for patients.

1. Introduction

Lung cancer is one of the most common cancers worldwide, with a high mortality rate, accounting for 18% of all cancer-related deaths. Smoking is the main cause of lung cancer (Klupczynska-Gabryszak et al., 2024). Lung cancer is a heterogeneous disease, mainly divided into non-small cell lung cancer (NSCLC) and small cell lung cancer (SCLC) (Wen et al., 2024). Non-small cell lung cancer, which accounts for 85% of lung cancer cases, includes adenocarcinoma (ADC), squamous cell carcinoma (SCC), and large cell carcinoma (LCC); The remaining 15% are small cell lung cancers with neuroendocrine features.

In the era of personalized medicine, the diagnosis and precise classification of lung cancer rely heavily on cytological and histological typing, which is usually evaluated microscopically by standard histochemical staining and auxiliary immunohistochemical staining. Molecular assays are also essential for the targeting of personalized therapies and for monitoring stratification of patient response to targeted and immunotherapy (Anand et al., 2020).

According to guidelines from the College of American Pathologists, the International Association for the Study of Lung Cancer, and the Association for Molecular Pathology (Rodriguez-Canales et al., 2016; Malapelle et al., 2021), patients with advanced lung adenocarcinoma should be tested for EGFR mutations, ALK and ROS1 rearrangements, BRAFV600E, RET rearrangements, MET exon 14 hops, KRAS mutations, and NTRK1-3 fusions (Wen et

* Corresponding Author.
Email Address: kanakarn_ph@rmutto.ac.th (K. Phanniphong)
https://doi.org/10.21833/ijaas.2025.11.003
Corresponding author's ORCID profile:
https://orcid.org/0000-0003-0569-0373

al., 2024; Lindeman et al., 2018). For advanced non-neuroendocrine carcinoma, detection of PD-L1 expression status is important because patients with PD-L1 tumor proportion score (TPS) ≥ 50% are eligible for first-line treatment with the anti-PD-L1 therapy pembrolizumab. The expression status of PD-L1 and ALK can be detected by immunohistochemistry. Currently, progress is being made in the detection of reflex order in lung cancer, which underscores the importance of collaboration among pathologists (Osmani et al., 2018; Udall et al., 2018; Kim et al., 2017; Wynes et al., 2014). Although reflection detection is not yet feasible in many laboratories, it can provide additional valuable information, detect rare molecular changes, and shorten the detection cycle (Anand et al., 2020; Zacharias et al., 2021).

Over the past decade, deep learning (DL) methods, particularly convolutional neural networks (CNNS), have shown increasing value in pathology. The DL model can overcome limitations such as a global shortage of pathologists, diagnostic subjectivity, and inter-observer and intra-observer variability. Recent advances in lung cancer pathology utilize the image analysis potential of H&E whole-film imaging (WSIs) to diagnose cancer (Wang et al., 2019; Baxi et al., 2022). Considering that material for 70% of patients with advanced, unresectable lung cancer is limited to small biopsies and cytological specimens, the DL approach can guide diagnosis with high precision, reduce the additional special staining required for differential diagnosis, and preserve limited material for molecular testing and oncology studies (Bubendorf et al., 2017).

Traditional methods of pathology image analysis rely on hand-crafted features and traditional machine learning methods such as support vector machines and random forests. Although these techniques have had some success, they are often inadequate in dealing with complex patterns and textures in pathological images (Bubendorf et al., 2017). The emergence of deep learning, particularly convolutional neural networks, has revolutionized the field of medical imaging by enabling high-precision automatic feature extraction and classification (Iqbal et al., 2024).

In recent years, Transformers models originally developed for natural language processing tasks have shown great potential in image analysis because of their ability to capture remote dependencies and contextual information through self-attention mechanisms (Ouzzani et al., 2016). Combining Transformers with CNN can further enhance feature extraction capabilities by focusing on relevant regions in pathological images, thereby improving the accuracy of diagnostic and prognostic models (Jain et al., 2022).

Digital pathology uses full-section scanning technology to convert cell and histopathological slides into high-resolution images known as Whole Slide images (WSI). This technology was originally developed for research, but is now widely used in clinical practice. Through imaging and processing of high-magnification images, it not only simplifies the daily work of pathologists, enhances diagnostic accuracy, reduces misdiagnosis due to technical differences, saves diagnostic time, supports remote consultation and information sharing, and accelerates the process of obtaining external expert opinions (Kanavati et al., 2020; Moranguinho et al., 2021; Tsuneki and Kanavati, 2022). The digital management of pathological sections was realized. Still, the number of cases is growing far faster than specialists can be trained, and it is uneconomical to devote valuable human resources to repetitive image recognition and diagnostic work. In recent years, with the development of artificial intelligence technology and the popularization of digitized pathological sections, digital pathology can gradually meet the needs of doctors for accurate detection, classification, and prediction of pathological images (Civit-Masot et al., 2022; Kanavati et al., 2021).

The purpose of this study is to explore and optimize the classification model of lung cancer pathological images, in order to improve the efficiency and accuracy of the construction of pathological classification and prognosis models. By introducing the spatial-channel attention (SCA) mechanism, to enhance the application of deep learning technology in the analysis of lung cancer pathological images. In the comparison of model performance, the SCA-ResNet model is superior to the traditional ResNet-50 model in accuracy, recall rate, specificity, F1 score, and Kappa coefficient. ROC curve analysis also showed that the SCA-ResNet model performed better in the task of classifying lung cancer pathological images, especially in the diagnostic efficiency of different cancer grades. Through these studies, this paper aims to provide a more accurate and efficient model for the classification of pathological images and help the diagnosis and treatment of lung cancer.

By achieving these goals, this study aims to promote innovation in lung cancer pathological image analysis technology and provide more powerful technical support for precision medicine and personalized treatment.

2. Methodology

The methodology part of this study elaborates on the overall process of using deep learning and Transformer technology to extract features and build a pathological grade and prognosis model of lung cancer. The key steps include data acquisition, pre-processing, model design and training, evaluation, and verification.

2.1. Feature extraction based on pathological diagnostic criteria

Deep learning networks rely on learning cell features in pathological images to determine the benign and malignant grade of lung cancer nodules. The pathological diagnostic criteria of lung cancer can be divided into 4 levels, and the pathological

images of lung cancer are professionally diagnosed and graded by the pathologists of the Affiliated Cancer Hospital of Fudan University in Shanghai. The pathological images and deep learning features of lung cancer are shown in Tables 1 and 2.

Pathologists grade pathological samples according to the pathological diagnostic criteria of lung cancer. However, the computer cannot directly extract the cellular features of pathological images according to the grading criteria. The abstract features of the images need to be transformed into natural features such as brightness, edge, texture, and color that can be recognized by the computer. Therefore, it is necessary to simplify the pathological diagnosis criteria of lung cancer into the feature classification criteria that can be learned by the computer, as shown in Table 1. A lot of information is difficult to quantify numerically, so part of the information is displayed graphically, and part of the descriptive information is shown in Fig. 1.

2.2. Improving the ResNet-50 network

In 2015, Microsoft proposed the basic Network architecture of the ResNet (Residual Network) model, of which RESNET-50 is the most commonly used one. The ResNet model solves the problem of gradient disappearing and gradient explosion in deep neural network training through residual connection, which enables the network to learn image features at a deeper level.

Some of the attention mechanisms in the ResNet-50 network have certain limitations in processing lung cancer pathological images. The spatial distribution of cancer cells in lung cancer pathological images and the relationship between cancer cells and surrounding tissues are of great significance to the pathological diagnosis results, but the original attention mechanism may pay too much attention to the channel information and ignore the accuracy of cancer cell location information. To solve this problem, this study introduces the Spatial-Channel Attention (SCA) mechanism.

The SCA attention mechanism considers both spatial and channel information. In the spatial dimension, it highlights the features of cancer cells and their surrounding key tissue regions by weighting the features of different regions. In terms of channel dimension, the importance of different characteristic channels is re-evaluated. Specifically, the SCA attention mechanism first partitions the input feature graph in spatial dimensions, computes feature statistics for each partition, and then generates spatial attention weights based on this information.

At the same time, in the channel dimension, a similar method is used to generate channel attention weight. Finally, a comprehensive attention weight is obtained by combining the spatial attention weight and the channel attention weight and applied to the input feature map.

The transfer learning strategy is used to replace the original attention mechanism on the basis of the original ResNet-50 model network. This new model is called the improved ResNet-50, namely the SCA-ResNet model. The SCA attention mechanism structure is shown in Fig. 2. Among them, r is used to control the size of the space partition and other related attributes. The SCA attention mechanism encodes location information and channel relationships, including spatial information embedding, channel information embedding and synthetic attention generation.

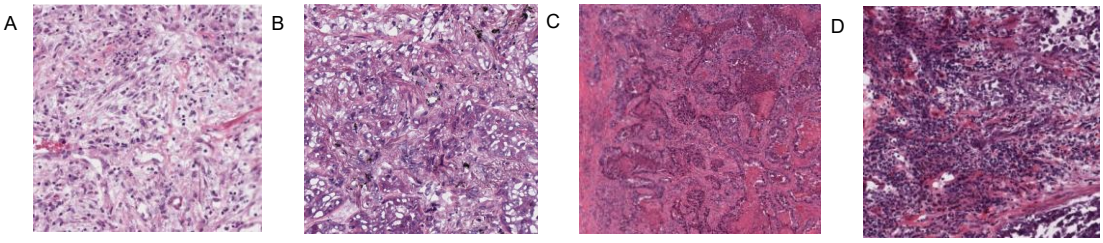

Fig. 1: Pathological images of lung cancer: (A) stage I, (B) stage II, (C) stage III, (D) stage IV

Table 1: Classification criteria of lung cancer

Cancer grade	Pathologist Diagnostic Criteria	Computer Feature Classification Standard
I	Small tumor confined to lung; no lymph node or distant metastasis. Well-differentiated cells; morphology close to normal; rare mitosis.	Brightness: Uniform, minimal difference from normal tissue. Edges: Clear and regular boundaries. Texture: Simple, regular. Color: Similar to normal cells, evenly distributed.
II	Tumor shows local growth, may invade nearby tissue; no metastasis. Moderately differentiated cells; mitosis more frequent than grade I.	Brightness: Slightly lower than normal tissue; some darker regions. Edges: Begin to appear irregular, mildly blurred. Texture: More complex, locally disturbed. Color: Increased variation from normal cells.
III	Large tumor, possible regional lymph node metastasis; poor cell differentiation; atypical mitosis observed.	Brightness: Significantly lower, uneven with interleaved dark and bright areas. Edges: Irregular, blurred, with protrusions or dents. Texture: Very complex and chaotic. Color: Strongly different from normal cells, uneven distribution.
IV	Distant metastasis (e.g., brain, bone). Very poor differentiation; severe cell deformation; many atypical mitoses.	Brightness: Extremely uneven with large dark areas. Edges: Highly irregular and invasive; boundary unclear. Texture: Disorganized, loss of normal structure. Color: Highly heterogeneous, complex variations.

1. Spatial information embedding: In order to effectively capture the spatial information in lung cancer pathological images, the input feature map was divided into n partitions, where the size of each partition is $(\frac{H}{n}, \frac{W}{n})$ (assume that the height of the input feature map is H and the width is W). For each partition, its characteristic statistics are calculated using an average pooling operation. For the KTH partition, its average pooled characteristics are expressed as:

$$Z_{s,k} = \frac{1}{\frac{H}{n} \times \frac{W}{n}} \sum_{i=\frac{(k-1)H}{n}}^{\frac{kH}{n}} \sum_{j=\frac{(k-1)W}{n}}^{\frac{kW}{n}} x(i,j)$$

where, $x(i,j)$ represents the eigenvalue of the input feature map at position (i,j).

Through the above operation, the feature representation of n partitions is obtained $\{Z_s, 1, Z_s, 2, \ldots, Z_s, n\}$.

These features are then transformed using a fully connected layer (FC) to generate spatial attention weights. The input dimension of the fully connected layer is n, and the output dimension is n, and its transformation formula is as follows:

$$W_s = \partial(FC(Z_s))$$

where, $Z_s = [Z_s, 1, Z_s, 2, \ldots, Z_s, n]$, δ is the activation function. The sigmoid function is used here.

2. Channel information embedding: Similar to spatial information embedding, in terms of channel dimension, the input feature graph is firstly globally average-pooled to obtain a C-dimensional feature vector (assuming that the input feature graph has C channels), expressed as:

$$Z_c = \frac{1}{H \times W} \sum_{i=1}^{H} \sum_{j=1}^{W} x_c(i,j)$$

where, $X_c(i,j)$ represents the eigenvalue of the c channel in the input feature map at position (i,j).

This feature vector is then transformed using a fully connected layer to generate channel attention weights. The input dimension of the fully connected layer is C, and the output dimension is C, and its transformation formula is as follows:

$$W_c = \partial(FC(Z_c))$$

3. Comprehensive attention generation: A comprehensive attention weight w is obtained by combining the generated spatial attention weight W_s with the channel attention weight W_c. Here, the combination is performed by simple element multiplication, that is:

$$W = W_s ! W_c$$

where, ! indicates the element multiplication operation.

Finally, the comprehensive attention weight w is applied to the input feature graph x, and the feature graph y after the SCA attention mechanism processing is obtained. The formula is:

$$y = w.x$$

SCA attention mechanism structure:

- Input layer: Input feature graph x, whose dimensions are (C, H, W).
- Spatial information embedding layer: the input feature map is divided into spatial partitions, the feature statistics of each partition are calculated, and the spatial attention weight W_s is obtained after the transformation of the fully connected layer.
- Channel information embedding layer: The input feature map is globally average-pooled, and the channel attention weight w is obtained after the transformation of the full connection layer W_c.
- Comprehensive attention generation layer: The comprehensive attention weight w is obtained by multiplying the spatial attention weight and the channel attention weight.
- Output layer: The comprehensive attention weight is applied to the input feature graph to obtain the output feature graph y.

The parameter n (number of partitions) is used to control the size of the space partition and other related attributes. For example, when n is larger, the spatial partition is smaller, and the spatial information can be captured more finely, but the computation amount will increase accordingly. When n is small, the space partition is large and the computation is small, but some spatial details may be lost.

2.3. Experimental indicators

All the experiments in this research have used Windows 10 to operate the system, a GeForce RTX 1650 graphics card, CUDA 11.0, Anaconda3 family Learn computing environment, and PyCharm IDE development environment. A neural network is built on the Pytorch framework to analyze the pathological images of thyroid cancer, conduct training, validation, and testing.

The performance of deep learning models in different tasks needs to be quantified. Horizontal comparison can only be made by conducting experiments on indicators. This study was conducted by precision, recall rate, specificity, F1-score, ROC curve, and Kappa coefficient to evaluate and test performance.

2.4 Data source

The data used in this paper are from the TCGA-LUAD lung cancer image dataset. (TCGA-LUAD is the pathological cohort of TCGA, which contains sequencing data and pathological image information.

LUAD RNA-seq data from patients with cancer genome atlas (https://portal.gdc.cancer.gov/), the dataset included 541 patients with 476 images. Basic information of the case is shown in Fig. 3.

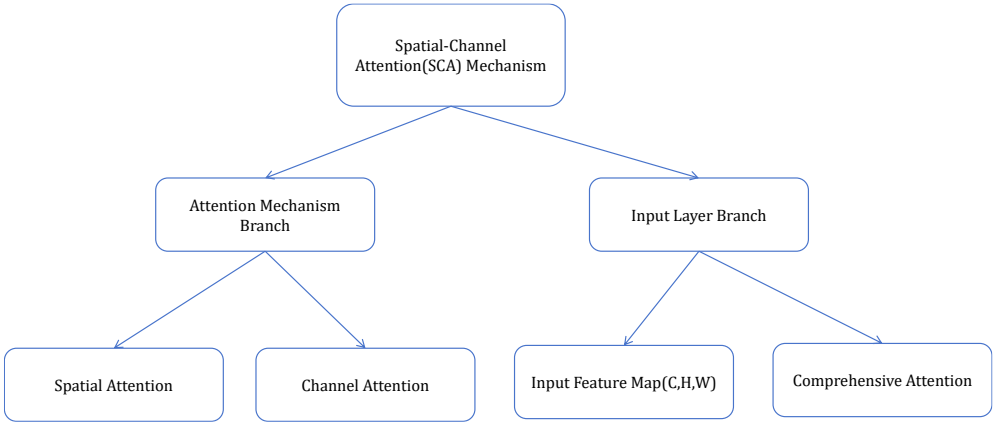

Fig. 2: Structure of the SCA mechanism

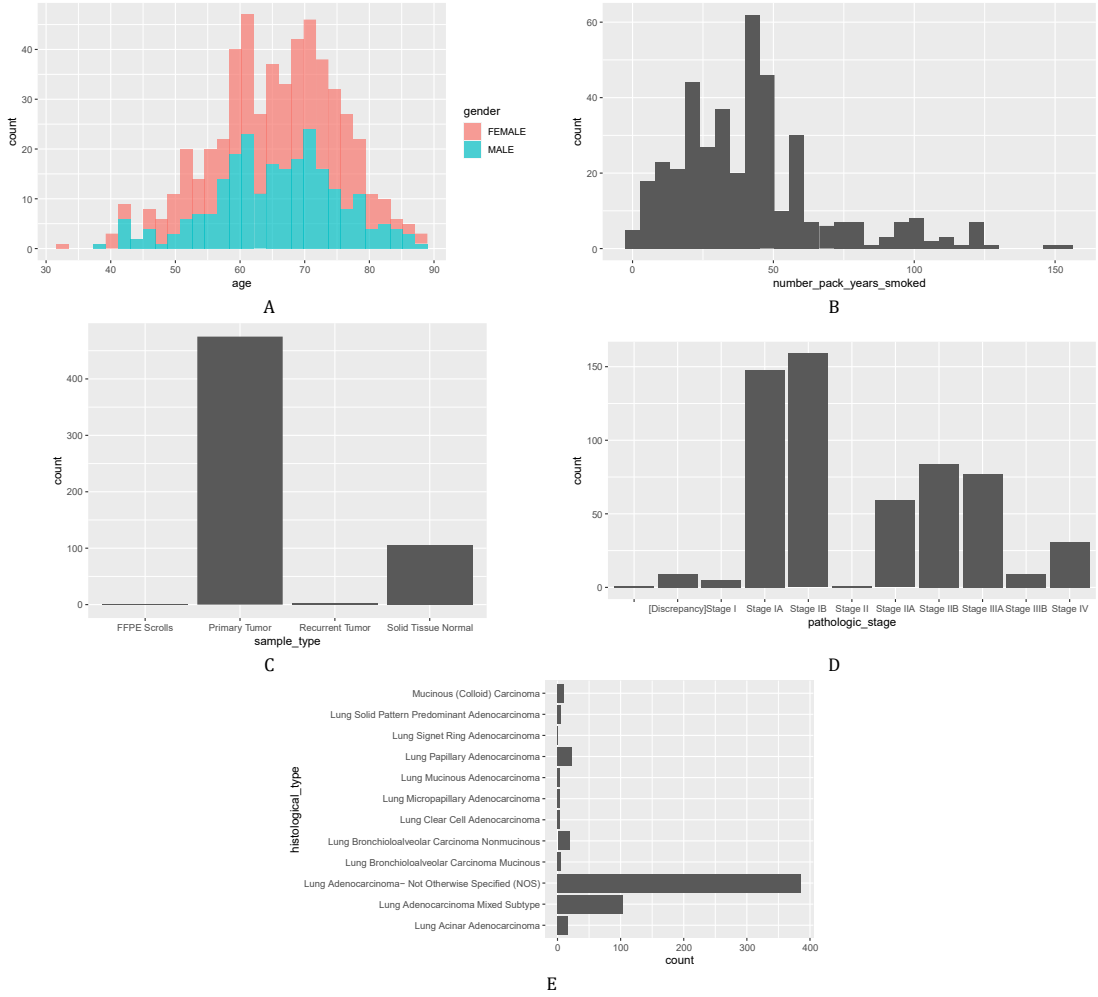

Fig. 3: Clinical and pathological characteristics: (A) age; (B) smoking years; (C) sample type; (D) pathologic stage; (E) histological type

3. Experimental results and analysis

3.1. Parameter optimization

The proper selection of hyperparameters is crucial for deep learning models, whose goal is to enable the models to learn data structures quickly while avoiding overfitting and underfitting. The optimized parameters usually include batch sample size, learning rate, parameters of different optimizers, etc. These parameters help the neural network convergence, thus improving the model performance. Limited by the number of lung cancer data sets, this study only divided some lung cancer pathological images for auxiliary diagnostic system testing. The remaining data sets are randomly divided into the training set, verification set, and test set of the neural network according to the ratio of 7:2:1, and the training set will be augmented and expanded. Next, optimization experiments will be

carried out for parameters such as learning rate, convolution kernel, batch sample size, and training set/verification set.

1. Learning rate optimization: First compares different initial learning rates (lr) and learning decay rate (lrf). In view of the large number of lung cancer grades, the average values of all grades were also calculated here, and the comparison results are shown in Table 2.

As can be seen from Table 3, the precision rate, recall rate, specificity, and F1 values of group 5 are significantly higher than those of the other 8 groups. Therefore, setting the initial lr to 0.01 and the lrf to 0.01 can obtain a network model with better effect, which is consistent with the conclusion of some existing studies that setting the initial learning rate to 0.01 has a better effect.

2. Batch sample size optimization: The number of batch samples will affect the optimization degree and speed of the model. Due to the limitation of computer performance in this study, the batch size cannot be greater than 32. The impact of batch size on the network is shown in Table 3.

Table 2: Comparison among different learning rates and learning decay rates

Learning rate and learning decay rate	Lost value	Precision rate	Recall rate	specificity	F1 score
lr = 0.001; lrf = 0.1	0.235	0.920	0.917	0.980	0.918
lr = 0.001; lrf = 0.01	0.235	0.919	0.918	0.981	0.917
lr = 0.001; lrf = 0.001	0.243	0.911	0.910	0.979	0.910
lr = 0.01; lrf = 0.1	0.071	0.940	0.930	0.985	0.935
lr = 0.01; lrf = 0.01	0.073	0.942	0.932	0.986	0.936
lr = 0.01; lrf = 0.001	0.079	0.940	0.930	0.985	0.935
lr = 0.1; lrf = 0.1	0.503	0.803	0.790	0.950	0.788
lr = 0.1; lrf = 0.01	0.380	0.893	0.889	0.970	0.888
lr = 0.1; lrf = 0.001	0.352	0.895	0.890	0.972	0.890

Table 3: Comparison among different batch sizes

Batch size	Lost value	Precision rate	Recall rate	specificity	F1 score
4	0.320	0.900	0.898	0.980	0.899
8	0.237	0.911	0.910	0.982	0.910
16	0.122	0.952	0.951	0.990	0.950
32	0.100	0.944	0.943	0.988	0.943

It can be seen from Table 4 that when the number of iterations is fixed, the larger batch size has the lowest loss value, but the accuracy rate is not optimal. When batch size = 16, the loss value is small, and other indicators are at the highest value, so when batch size = 16, the performance of the model is the best.

3. Other optimization: Some parameters are modified when it is not recommended to train the model, such as beta 1 set to 0.9 and beta 2 set to 0.999 in the Adam optimizer. In addition to the above parameters, there are also some common parameters that need to be optimized and adjusted by researchers, such as the convolution kernel size and training set/verification set ratio.

Convolution kernel size: Horizontal comparison of convolution kernel sizes of 3×3, 5×5, and 7×7 is carried out, and the comparison results are shown in Table 4.

In the case of little difference in loss values, the 7×7 convolution kernel with a high accuracy rate is preferred.

Table 4: Comparison among different convolutional kernels

Convolution kernel size	Lost value	Precision rate	Recall rate	specificity	F1 score
3×3	0.150	0.930	0.932	0.981	0.943
5×5	0.145	0.935	0.935	0.982	0.946
7×7	0.140	0.940	0.952	0.982	0.948

Transfer learning: Transfer learning has a significant gain effect on most networks, which can improve the learning efficiency of the network. Table 5 shows the impact of transfer learning on deep learning networks. In this experiment, the pre-training weights trained on ImageNet were imported into the convolutional neural network to reduce the training time of a large number of lung cancer pathology data sets. The index values of the two experiments are close, but the number of training iterations with transfer learning is one-quarter of that without transfer learning.

Table 5: Effect of transfer learning on the network

Whether to use transfer learning	Lost value	Precision rate	Recall rate	specificity	F1 score
Yes	40	0.954	0.952	0.987	0.952
No	100	0.958	0.953	0.988	0.957

3.2. Experimental result

To evaluate the performance of the SCA-ResNet model on a lung cancer pathology image dataset, we conducted a series of experiments and compared it with the ResNet-50 model (Table 6). In the experiment, we recorded the changes of important

indicators such as precision rate, recall rate, specificity, and F1 score during model training.

In terms of accuracy rate, the accuracy data of the ResNet-50 model in the training process is 0.945, while the accuracy rate of the SCA-ResNet model reaches 0.960. It can be seen that the SCA-ResNet model has an improvement of 0.015 in accuracy. In terms of recall rate, the recall rate of the ResNet-50 model is 0.938, and that of the SCA-ResNet model is 0.972, which indicates that the SCA-ResNet model also shows an advantage of 0.034 in recall rate. In terms of the specificity index, the specificity of the ResNet-50 model was 0.964, and that of the SCA-ResNet model was increased to 0.984, indicating that the SCA-ResNet model had a stronger ability to correctly identify negative samples. The F1 score combines the information of accuracy and recall rate. The F1 score of the ResNet-50 model is 0.951, and the F1 score of the SCA-ResNet model is 0.971, which further proves that the SCA-ResNet model is better than the ResNet-50 model in overall performance.

The ROC curve is also a key way to measure model performance. In the training process based on the lung cancer pathological image dataset in this study, the ROC curve comparison between the ResNet-50 and SCA-ResNet models showed that the closer the ROC curve was to the upper left corner, the lower the false positive rate and the higher the true positive rate of the classifier. The ROC curve of the SCA-ResNet model is closer to the upper left corner, and the area under the ROC curve of the SCA-ResNet model is larger than that of the ResNet-50 model, which further proves the superiority of the SCA-RESNET model in the lung cancer pathological image classification task.

In addition, the Kappa coefficient of the ResNet-50 model is 0.943, and that of the SCA-ResNet model is 0.952. The Kappa coefficient of the two models is at a higher level, but the Kappa coefficient of the SCA-ResNet model is 0.008 higher than that of the ResNet-50 model, which indicates that the predicted results of the SCA-ResNet model are more consistent with the actual classification results.

In summary, the SCA-ResNet model demonstrates superior performance across various metrics compared to the ResNet-50 model.

Table 6: Comparison of diagnostic efficiency

Cancer grade	ResNet-50				SCA-ResNet			
	Precision rate	Recall rate	specificity	F1 score	Precision rate	Recall rate	specificity	F1 score
I	0.957	0.937	0.951	0.932	0.986	0.987	0.992	0.983
II	0.932	0.912	0.933	0.932	0.975	0.982	0.994	0.961
III	0.947	0.961	0.987	0.977	0.957	0.977	0.977	0.977
IV	0.943	0.943	0.983	0.963	0.923	0.943	0.973	0.963
Average	0.945	0.938	0.964	0.951	0.960	0.972	0.984	0.971

The ROC curve is also an important way to measure the model. Figs. 4 and 5 show the ROC curve comparison between the ResNet-50 model and the improved SCA-ResNet during training based on the data set of this study. The closer the ROC curve is to the upper left corner, the lower the false positive rate and the higher the true positive rate of the classifier. As can be seen from Figs. 4 and 5, both models perform well, but the area under the total ROC curve of the improved SCA-ResNet is larger than that of the ResNet-50 model, which is why SCA-ResNet performs better.

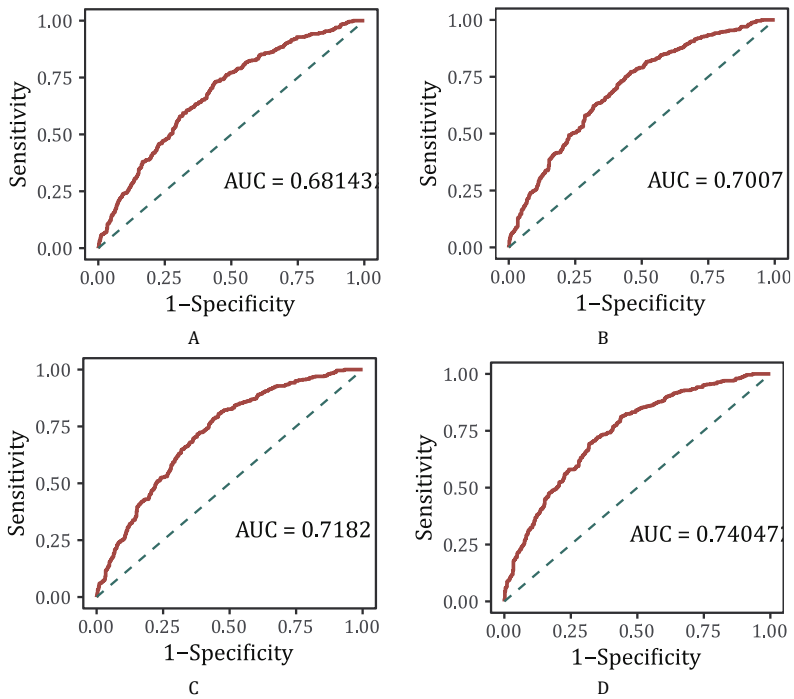

Fig. 4: ROC curves of ResNet-50: (A) first class; (B) second class; (C) third class; (D) fourth class

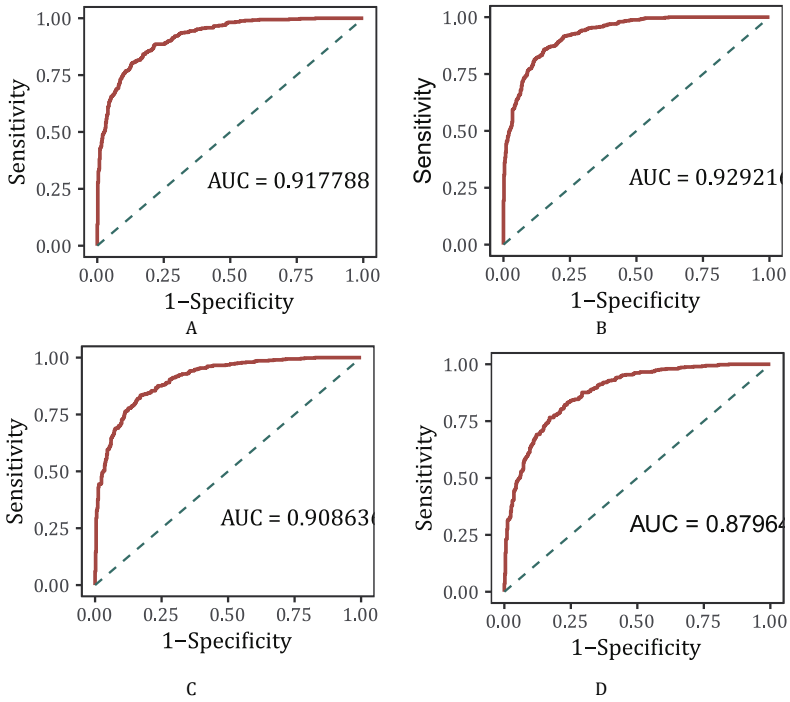

Fig. 5: ROC curves of SCA-ResNet: (A) first class; (B) second class; (C) third class; (D) fourth class

4. Discussion

The optimization of hyperparameters in this study significantly enhances the convergence speed and overall performance of the neural networks. However, the limited number of lung cancer datasets constrains the ability to comprehensively cover all potential data scenarios, which may result in some limitations in the parameter optimization outcomes. Furthermore, the parameter optimization process only explored a limited range of values, suggesting the possibility of even better parameter combinations that were not identified in this study.

Compared to the ResNet-50 model, SCA-ResNet introduces a spatial-channel attention mechanism, enabling the model to focus more on critical channels and spatial regions, thereby improving feature utilization. By dynamically adjusting feature weights, it enhances important features and suppresses redundant information, which enhances the model's feature representation capability and generalization performance. This allows the model to process complex pathological images more effectively and distinguish various key features, ultimately improving its ability to accurately classify different cancer grades.

The SCA-ResNet model constructed in this study shows significant potential for application in the early diagnosis of lung cancer. Accurate classification and analysis of pathological images can provide doctors with precise diagnostic references, thereby improving the efficiency and accuracy of lung cancer diagnosis.

To further enhance the model's performance, future research could focus on collecting a more extensive dataset of lung cancer pathology images to address the limitations imposed by the current dataset size. Exploring other advanced model structures or optimization algorithms could also lead to improved performance in lung cancer pathological image analysis tasks. Additionally, integrating the model with other clinical information, such as patient genetic data and clinical symptoms, could help build a more comprehensive lung cancer diagnosis system.

The limited dataset size may not represent the full diversity of lung cancer pathological images, potentially affecting the generalizability of the results. Assumptions made during parameter optimization and model training, such as the fixed range of hyperparameters, may also limit the scope of the findings. Future research should consider these threats and aim to validate the model's performance across more diverse and extensive datasets.

4.1. Future scope

Future research should focus on addressing the limitations identified in this study by expanding the dataset and exploring a broader range of hyperparameters. Additionally, investigating the integration of the SCA-ResNet model with other advanced techniques, such as ensemble learning and hybrid models, could further enhance its performance. The potential application of the model in other types of cancer or medical image analysis tasks also warrants exploration. The development of user-friendly software tools based on the SCA-ResNet model could facilitate its adoption in clinical settings, ultimately contributing to improved patient outcomes. Pan et al. (2025) found that the use of a new architecture, VcaNet, integrating the visual converter (ViT) with the fusion channel and spatial attention module (CBAM), aims to enhance 3D brain tumor segmentation. In the future, attempts can be

made to integrate SCA with Vision Transformers for clinical 3D pathology to lay the foundation for the future development of medical imaging.

List of abbreviations

ADC	Adenocarcinoma
ALK	Anaplastic lymphoma kinase
BRAF	B-Raf proto-oncogene
CBAM	Convolutional Block Attention Module
CNNS	Convolutional neural networks
CUDA	Compute Unified Device Architecture
EGFR	Epidermal growth factor receptor
FC	Fully connected layer
FISH	Fluorescence in situ hybridization
H&E	Hematoxylin and eosin
IDE	Integrated development environment
KRAS	Kirsten rat sarcoma virus
LCC	Large cell carcinoma
lr	Learning rate
lrf	Learning rate decay factor
MET	MET proto-oncogene
NSCLC	Non-small cell lung cancer
NTRK	Neurotrophic tyrosine receptor kinase
PD-L1	Programmed death-ligand 1
RESNET	Residual Network
RNA-seq	Ribonucleic acid sequencing
ROC	Receiver operating characteristic
ROS1	ROS proto-oncogene 1
SCA	Spatial-channel attention
SCA-ResNet	Spatial-channel attention Residual Network
SCC	Squamous cell carcinoma
SCLC	Small-cell lung cancer
TCGA-LUAD	The Cancer Genome Atlas Lung Adenocarcinoma
TPS	Tumor proportion score
VcaNet	Vision Transformer with fusion channel and spatial attention module
ViT	Vision Transformer
WSIs	Whole-slide images

Funding

This research was supported by funding from Guangzhou Huashang College Natural Science Fund of young scholars under grant 2021HSQX53 and Guangzhou Huashang College tutorial system project fund 2022HSDS01. The funding bodies played no role in the design of the study, collection, analysis, or interpretation of data, nor in the writing of the manuscript or the decision to submit it for publication. The authors declare that the content of this manuscript reflects their independent academic work and judgment.

Compliance with ethical standards

Ethical considerations

This study was conducted using the publicly available TCGA-LUAD dataset. All patient data in this resource is fully de-identified and made available with informed consent under controlled access procedures.

Conflict of interest

The author(s) declared no potential conflicts of interest with respect to the research, authorship, and/or publication of this article.

References

Anand K, Phung TL, Bernicker EH, Cagle PT, Olsen RJ, and Thomas JS (2020). Clinical utility of reflex ordered testing for molecular biomarkers in lung adenocarcinoma. Clinical Lung Cancer, 21(5): 437-442. https://doi.org/10.1016/j.cllc.2020.05.007 **PMid:32600793**

Baxi V, Edwards R, Montalto M, and Saha S (2022). Digital pathology and artificial intelligence in translational medicine and clinical practice. Modern Pathology, 35(1): 23-32. https://doi.org/10.1038/s41379-021-00919-2 **PMid:34611303 PMCid:PMC8491759**

Bubendorf L, Lantuejoul S, de Langen AJ, and Thunnissen E (2017). Nonsmall cell lung carcinoma: Diagnostic difficulties in small biopsies and cytological specimens. European Respiratory Review, 26(144): 170007. https://doi.org/10.1183/16000617.0007-2017 **PMid:28659503 PMCid:PMC9488516**

Civit-Masot J, Bañuls-Beaterio A, Domínguez-Morales M, Rivas-Perez M, Muñoz-Saavedra L, and Corral JMR (2022). Non-small cell lung cancer diagnosis aid with histopathological images using explainable deep learning techniques. Computer Methods and Programs in Biomedicine, 226: 107108. https://doi.org/10.1016/j.cmpb.2022.107108 **PMid:36113183**

Iqbal MS, Heyat MBB, Parveen S et al. (2024). Progress and trends in neurological disorders research based on deep learning. Computerized Medical Imaging and Graphics, 116: 102400. https://doi.org/10.1016/j.compmedimag.2024.102400 **PMid:38851079**

Jain DK, Lakshmi KM, Varma KP, Ramachandran M, and Bharati S (2022). Lung cancer detection based on kernel PCA-convolution neural network feature extraction and classification by fast deep belief neural network in disease management using multimedia data sources. Computational Intelligence and Neuroscience, 2022: 3149406. https://doi.org/10.1155/2022/3149406 **PMid:35669646 PMCid:PMC9167006**

Kanavati F, Toyokawa G, Momosaki S et al. (2020). Weakly-supervised learning for lung carcinoma classification using deep learning. Scientific Reports, 10: 9297. https://doi.org/10.1038/s41598-020-66333-x **PMid:32518413 PMCid:PMC7283481**

Kanavati F, Toyokawa G, Momosaki S et al. (2021). A deep learning model for the classification of indeterminate lung carcinoma in biopsy whole slide images. Scientific Reports, 11: 8110. https://doi.org/10.1038/s41598-021-87644-7 **PMid:33854137 PMCid:PMC8046816**

Kim H, Kwon HJ, Park SY, Park E, and Chung JH (2017). PD-L1 immunohistochemical assays for assessment of therapeutic strategies involving immune checkpoint inhibitors in non-small cell lung cancer: A comparative study. Oncotarget, 8(58): 98524–98532. https://doi.org/10.18632/oncotarget.21567 **PMid:29228707 PMCid:PMC5716747**

Klupczynska-Gabryszak A, Daskalaki E, Wheelock CE et al. (2024). Metabolomics-based search for lung cancer markers among patients with different smoking status. Scientific Reports, 14: 15444. https://doi.org/10.1038/s41598-024-65835-2 **PMid:38965272 PMCid:PMC11224321**

Lindeman NI, Cagle PT, Aisner DL et al. (2018). Updated molecular testing guideline for the selection of lung cancer patients for

treatment with targeted tyrosine kinase inhibitors: Guideline from the College of American Pathologists, the International Association for the Study of Lung Cancer, and the Association for Molecular Pathology. Archives of Pathology and Laboratory Medicine, 142(3): 321-346.
https://doi.org/10.5858/arpa.2017-0388-CP
PMid:29355391

Malapelle U, Leprieur EG, Kamga PT, Chiasseu MT, and Rolfo C (2021). Emerging biomarkers for NSCLC: Recent advances in diagnosis and therapy. Frontiers in Oncology, 11: 694578.
https://doi.org/10.3389/978-2-88966-915-8

Moranguinho J, Pereira T, Ramos B, Morgado J, Costa JL, and Oliveira HP (2021). Attention based deep multiple instance learning approach for lung cancer prediction using histopathological images. In the 43rd Annual International Conference of the IEEE Engineering in Medicine and Biology Society, IEEE, Mexico City, Mexico: 2852-2855.
https://doi.org/10.1109/EMBC46164.2021.9631000
PMid:34891842

Osmani L, Askin F, Gabrielson E, and Li QK (2018). Current WHO guidelines and the critical role of immunohistochemical markers in the subclassification of non-small cell lung carcinoma (NSCLC): Moving from targeted therapy to immunotherapy. Seminars in Cancer Biology, 52: 103-109.
https://doi.org/10.1016/j.semcancer.2017.11.019
PMid:29183778 PMCid:PMC5970946

Ouzzani M, Hammady H, Fedorowicz Z, and Elmagarmid A (2016). Rayyan: A web and mobile app for systematic reviews. Systematic Reviews, 5: 210.
https://doi.org/10.1186/s13643-016-0384-4
PMid:27919275 PMCid:PMC5139140

Pan D, Shen J, Al-Huda Z, and Al-Qaness MA (2025). VcaNet: Vision Transformer with fusion channel and spatial attention module for 3D brain tumor segmentation. Computers in Biology and Medicine, 186: 109662.
https://doi.org/10.1016/j.compbiomed.2025.109662
PMid:39813745

Rodriguez-Canales J, Parra-Cuentas E, and Wistuba II (2016). Diagnosis and molecular classification of lung cancer. In: Reckamp K (Ed.), Lung cancer: Treatment and research: 25-46. Springer, Cham, Switzerland.
https://doi.org/10.1007/978-3-319-40389-2_2
PMid:27535388

Tsuneki M and Kanavati F (2022). Weakly supervised learning for multi-organ adenocarcinoma classification in whole slide images. PLOS ONE, 17(11): e0275378.
https://doi.org/10.1371/journal.pone.0275378
PMid:36417401 PMCid:PMC9683606

Udall M, Rizzo M, Kenny J, Doherty J, Dahm S, Robbins P, and Faulkner E (2018). PD-L1 diagnostic tests: A systematic literature review of scoring algorithms and test-validation metrics. Diagnostic Pathology, 13: 12.
https://doi.org/10.1186/s13000-018-0689-9
PMid:29426340 PMCid:PMC5807740

Wang S, Yang DM, Rong R et al. (2019). Artificial intelligence in lung cancer pathology image analysis. Cancers, 11(11): 1673.
https://doi.org/10.3390/cancers11111673
PMid:31661863 PMCid:PMC6895901

Wen T, Zhang X, Gao Y, Tian H, Fan L, and Yang P (2024). SOX4-BMI1 axis promotes non-small cell lung cancer progression and facilitates angiogenesis by suppressing ZNF24. Cell Death and Disease, 15: 698.
https://doi.org/10.1038/s41419-024-07075-w
PMid:39349443 PMCid:PMC11442842

Wynes MW, Sholl LM, Dietel M et al. (2014). An international interpretation study using the ALK IHC antibody D5F3 and a sensitive detection kit demonstrates high concordance between ALK IHC and ALK FISH and between evaluators. Journal of Thoracic Oncology, 9(5): 631-638.
https://doi.org/10.1097/JTO.0000000000000115
PMid:24722153 PMCid:PMC4186652

Zacharias M, Absenger G, Kashofer K et al. (2021). Reflex testing in non-small cell lung carcinoma using DNA-and RNA-based next-generation sequencing: A single-center experience. Translational Lung Cancer Research, 10(11): 4221–4234.
https://doi.org/10.21037/tlcr-21-570
PMid:35004252 PMCid:PMC8674594